Laser fabrication of Cu nanoparticles based nanofluid with enhanced thermal conductivity: experimental and molecular dynamics studies

T. Khamliche[a,b,e,*], S. Khamlich[a,b,c*], M.K. Moodley[d], B.M. Mothudi[e], M. Henini[a,b,f], M. Maaza[a,b]

[a]*UNESCO-UNISA Africa Chair in Nanosciences-Nanotechnology, PO Box 392, Pretoria-South Africa*
[b]*Nanosciences African Network (NANOAFNET), iThemba LABS-National Research Foundation, PO Box 722, Somerset West, Western Cape Province, South Africa*
[c]*Nanoenergy for Sustainable Development in Africa (NESDAF), P.O. Box 362, Western Cape, 7139, South Africa*
[d]*School of Chemistry and Physics, University of KwaZulu-Natal, Durban 4001, South Africa*
[e]*Department of Physics, College of Science, Engineering and Technology, University of South Africa, Private Bag X6, Florida 1710, Johannesburg, South Africa*
[f]*School of Physics and Astronomy, The University of Nottingham, University Park, Nottingham NG7 2RD, UK*

ABSTRACT

Nanofluids are engineered colloidal suspensions of solid nanoparticles in aqueous and non-aqueous base fluids with enhanced thermo-physical characteristics compared to conventional heat transfer fluids (HTFs). In this study, we report on the fabrication of copper nanoparticles-ethylene glycol (CuNPs-EG) nanofluid by using a simple one-step pulsed Nd:YAG laser ablation method to ablate the surface of a pure copper target in EG base fluid under ambient conditions. Structural and morphological analysis confirmed the fabrication of pure spherical shaped CuNPs with average diameter of ~ 7 nm. Thermal conductivity (k) investigations of CuNPs-EG nanofluid were conducted by using a computational approach where Equilibrium Molecular Dynamics (EMD) simulations integrated with Green-Kubo (EMD-GK) method was used. The obtained EMD-GK results for k were confirmed experimentally through a guarded hot-plate technique within the temperature ranges of 298 – 318 K. Interestingly, a relative enhancement (η) in the percentage of thermal conductivity of CuNPs-EG nanofluids obtained after an ablation time t_a = 5 mins was 15 % at 318 K, while sample obtained after t_a = 30 mins showed an enhancement of ~ 24 % in thermal conductivity. These obtained results confirmed the suitability of using a laser based ablation method to fabricate highly efficient nanofluids which could be used as alternatives for conventional HTFs in various heat transfer applications.

Keywords:
Nanofluid, laser ablation, thermal conductivity, nanoparticles, heat transfer

[*]Corresponding Authors : T. Khamliche & S. Khamlich
E-mail addresses: tkhamliche49@gmail.com, skhamlich@nesdaf.com

1. Introduction

Nanoparticles are nanosized materials with sizes ranging from 1 to 100 nm [1]. The unique characteristics of materials at the nano-size scale make them attractive, in particular, with respect to their outstanding thermo-physical properties when compared with bulk materials [2,3]. The rapid development and research in nanotechnology has led to the development of new classes of advanced HTFs or nanofluids where nanoparticles are added to the base fluid for better heat transfer and efficiency [4,5]. Additionally, the intrinsically high thermal conductivity of metallic nanoparticles allow them to be used as nano-fillers in conventional HTFs such as H_2O, oils, and ethylene glycol (EG) to enhance their thermo-physical properties which could lead to the design and development of heat transfer devices with high efficiency and compactness [6]. The significant enhancement in the thermal conductivity (k) of nanofluids was reported for a significant number of nanoparticles (metallic or metal oxides) containing nanofluids [4-8]. This observed enhancement indicated a great potential for nanofluids to revolutionize technologies that are dependent on the performance of HTFs [9]. Despite the confirmed high thermo-physical performances of nanofluids, the challenges of meeting the industrial demand have forced researchers to find new ways and to adopt cost-effective fabrication methods to allow the creation of uniformly dispersed and stable suspensions of metallic nanoparticles in liquids [10].

Several methods to synthesis and fabricate nanofluids based on metallic nanoparticles were developed, including wet chemical [11], photochemical [12], electrochemical [13] and radiolysis reduction [14]. Recently, a new method to fabricate nanofluids was used. In this method, ultrafast pulsed laser ablation of solid materials in liquids showed great potential as an alternative method for preparing nanoparticles based nanofluids [8,15]. In addition, due to its high effectiveness, this technique was intensively studied and investigated because of the

numerous advantages and versatility of laser materials processing, including nanostructured materials fabrication [16]. Compared to other methods, particularly chemical methods, ultrafast pulsed laser ablation (UPLA) of metallic bulk targets in liquids, is a simple method that normally operates in aqueous and non-aqueous solutions under ambient conditions. High-power pulsed laser ablation in a liquid medium was first described in 1987 by P.P. Patil et al. who fabricated metastable iron oxide at a liquid-solid interface where aqueous oxidation of iron was formed [17]. The mechanisms underlying the process of target surface evaporation consist in the fact that the temperature of the target material is raised locally due to the high-intensity laser beam accompanied with increased light absorption at the surface [16]. The most attractive aspect of laser ablation of solid targets in liquids is the simplicity, low environmental impact, and the practical approach to nanofluids design and engineering for different HTFs industrial applications [18]. Additionally, nanoparticles with different phases, compositions, and morphologies could be obtained when the experimental setup of laser ablation in liquids is tailored to produce the preferred nanomaterial structure [16]. However, in terms of other preparation methods, laser ablation incurs high investment costs because of the high price of laser systems to be economically convenient for large-scale production of nanoparticles based nanofluids [19]. Moreover, the formation of nanoparticles during the ablation process is accomplished by condensation of the ablated material ejected from the surface of the target as a result of the interaction of the laser beam with the target [20]. Amongst the variety of metallic nanoparticles, noble metals such as gold (Au) and silver (Ag) have been extensively studied due to their strong interaction with visible light through the collective oscillation of the conduction band electrons confined to the nanoscale structure of the nanoparticles [21]. In addition to Au and Ag, Copper (Cu) nanoparticles (CuNPs) also attracted attention due to their catalytic [22], electrolytic [23], and thermo-physical properties [24]. The formation of nanoparticles with different shapes and structures when a solid metal

target is irradiated by pulsed Nd:YAG laser in liquids has been reported previously [25-28].

Recently, molecular dynamics (MD) simulations showed great potential in determining the thermo-physical characteristics of nanofluids with acceptable predictions [29-34]. Using numerical simulations methods in combination with experimental techniques, have been proven to increase the understanding of nanomaterials and nanofluids [30-33]. MD simulations are conducted based on solving basic Newton's laws of motion for systems of interacting particles to provide significant insights into the atomic level of a material. The simulations can therefore identify, clarify, and probe the major mechanisms at a nano-scale level. By using MD simulations methods, molecular mechanics force fields (i.e., interatomic potentials) are used to compute atomic trajectories, inter-particle forces and their potential energies. Hence, MD simulations are used and preferred by many researchers to study the thermophysical properties of materials due to its efficiency and versatility as a computer simulation method [34−36].

In this work, copper nanoparticles-ethylene glycol (CuNPs-EG) based nanofluid was prepared by a simple one-step pulsed Nd:YAG laser ablation of bulk copper (Cu) target in EG base fluid. This laser-based top-down nanofabrication strategy is an effective approach that proved its remarkable advantage over conventional solution chemistry or other physical methods. To confirm the suitability of using CuNPs-EG as an efficient heat transfer fluid, thermal conductivity (k) analysis were carried out by using a computational approach where equilibrium molecular dynamics (EMD) simulations integrated with Green-Kubo (EMD-GK) method was utilized. The obtained EMD-GK results for k were confirmed experimentally through a homemade guarded hot-plate apparatus at different temperatures ranging from 298 K to 318 K.

2. Experimental and computational details

2.1. Fabrication and characterization

The method of fabricating CuNPs-EG nanofluid via laser ablation of a solid Cu target in a base fluid (EG) is shown in figure 1. A Cu target, 10 mm in diameter and 3 mm thick (from Sigma-Aldrich, purity: 99%) was placed at the bottom of a glass-beaker filled with 20 mL of EG as shown in figure 1.a. A pulsed Nd:YAG laser with wavelength of 1064 nm, pulse duration of 20 ns and output energy of 120 mJ/pulse was utilized during the experiments. The laser source was operated at a repetition rate of 10 Hz. The pulsed laser beam was focused through a convex lens with a focal length of 300 mm placed above the beaker. The Cu target was placed at the bottom of the beaker and about 2 cm below the EG top surface. The structural investigations of the fabricated CuNPs-EG nanofluid were conducted using X-ray diffractometer "model Bruker AXS D8 Advance" with irradiation from K_α line of copper "λ=1.5406 Å". The morphology of the obtained CuNPs was studied using a Field Emission Transmission Electron Microscope (TEM) (Tecnai F20). For the simulations, to extract the thermal conductivity, *k*, of the fabricated CuNPs-EG nanofluid, the well-established equilibrium molecular dynamics (EMD) simulations integrated with Green-Kubo method was first used and confirmed experimentally by a homemade guarded hot-plate apparatus (see section 2.4 for a detailed description of the apparatus).

2.2. Mechanisms of CuNPs formation under pulsed Nd:YAG laser ablation in EG

The mechanisms underlying the process of solid Cu ablation in ethylene glycol (EG) are shown in figure 1. During the initial stage of the ablation process, the temperature of the target material is raised locally due to the multi-photons absorption process at the surface [16,37]. The irradiation of a metallic target through a liquid layer can drive a number of inter-related phenomena. Firstly, when the laser interacts with the Cu target (figure 1.b), a local

ultra-fast heating process will take place, leading to a huge increase in its temperature followed by melting and evaporation of the target. Consequently, a plasma plume is formed due to the expansion of the evaporated material (vapor of Cu atoms) (figure 1.b). Secondly, this laser-induced plasma will expand adiabatically to create a shock wave, which results in extra pressure and temperature [38,39]. Moreover, energy transformation occurs during the expansion and condensation of the plasma plume, which causes the formation of a thin layer of EG vapor (figure 1.c) [37-39]. This formed EG layer of vapor will also expand into a cavitation bubble, while the plasma plume enters a cooling phase and shrinks leading to a decrease in pressure and temperature [38] (figure 1.d). Furthermore, CuNPs are produced within the bubble once the laser-induced plasma is collapsed (figure 1.e). In the final stage, the cavitation bubble will also collapse enabling the CuNPs to be transferred to the base fluid to form CuNPs-EG based nanofluid (figure 1.f).

2.3. MD simulation details

2.3.1. CuNPs-EG nanofluid simulation system

In the present work, ethylene glycol (EG) was used as the base fluid in a simulation box (100 Å × 100 Å × 100 Å cubic box), which contains 10,000 atoms, with a copper nanoparticle (CuNP) at its center as shown in figure 2. The CuNP used for the MD simulations was spherical in geometry with a diameter of ~ 7 nm. In addition, the EG molecules are considered as a matrix with a chain-like structure [40,41], where the CuNP is embedded to form CuNP-EG nanofluid. Therefore, the designed nanofluid system can be simplified as infinite multiples of identical model systems consisting of a single sub-nanometer cluster of Cu atoms in liquid EG as shown in figure 2. All MD simulations were carried out using the large-scale atomic/molecular massively parallel simulator (LAMMPS). The initial configuration of the nanofluid system with periodic boundary conditions in a 3D-

computing domain was energy minimized for 1,000 steps and then equilibrated for 100 ps, in the canonical ensemble (NVT) with the Nose−Hoover thermostat where the particles number (N), volume (V) and temperature (T) are conserved. After system equilibrium at a fixed temperature and atmospheric pressure, the MD simulations were run with a time increment of 0.04 fs for 100,000 time steps. In general, five independent simulations have been performed to obtain each MD result and error estimation.

2.3.2. Interatomic interaction forces

In classical molecular dynamics (MD) simulations, atomic vibrations are calculated and simulated by solving Newton's equation of motion where interactions between atoms are described by different interatomic potentials and force fields [42]. As a result, the atoms of a system are allowed to interact with each other and various thermo-physical quantities such as energy, pressure, density, temperature, velocity and thermal conductivity are calculated at each time step [43]. Furthermore, using MD simulations to study nanofluids, all possible molecular and atomic interaction are considered for accurate and reliable calculations [34]. Therefore, to simulate the CuNPs-EG nanofluid, OPLS-AA force field [44] was used to model interaction between the EG molecules, and the basic model parameters were taken from Jorgensen's paper for carbohydrates (OPLS-AA) [45]. In addition, the Lennard Jones (LJ) potential was used for interatomic interaction between different atoms (i.e. C, H, O and Cu), which is given by:

$$\varphi(r_{ij}) = 4\varepsilon_{ij}\left[\left(\frac{\sigma_{ij}}{r_{ij}}\right)^{12} - \left(\frac{\sigma_{ij}}{r_{ij}}\right)^{6}\right] \quad (1)$$

where ε_{ij} is the depth of the potential well, σ_{ij} is the finite distance at which the pairwise potential is zero (values are listed in Table 1), and r_{ij} is the distance between atoms *i* and *j*.

Table 1 Lennard–Jones parameters for atomic interactions in CuNPs-EG nanofluid system.

Atom (i-j)	ε_{ij} (kcal.mol^{-1})	σ_{ij} (Å)
H-C	0.030	2.50
C-C	0.066	3.50
O-H	0.170	3.07
H-Cu	0.03396	1.335
O-Cu	0.06387	2.7172

For interactions between Cu atoms, an embedded atom model (EAM) potential was used [46]. In the EAM potential, the potential energy of an atom, *i*, is given by:

$$E_i = F_\alpha \left(\sum_{i \neq j} \rho_\beta \left(r_{ij} \right) \right) + \frac{1}{2} \sum_{i \neq j} U_{\alpha\beta} \left(r_{ij} \right) \tag{2}$$

where F_α is an embedding function that represents the energy required to place atom *i* of type α into the electron cloud, ρ_β is the contribution of the electron charge density from atom *j* of type β at the location of atom *i*, r_{ij} is the distance between atoms *i* and *j*, and $U_{\alpha\beta}$ is a pair-wise potential function.

2.3.3. Equilibrium Molecular Dynamics (EMD) simulation integrated with Green-Kubo method (EMD-GK) for the thermal conductivity calculations

In general, computing the thermal conductivity of materials through MD simulations is based on two approaches: equilibrium molecular dynamics (EMD) and non-equilibrium molecular dynamics (NEMD) [47]. Due to the advantages of EMD compared with NEMD [48], it was adapted in our study to investigate and predict the thermal conductivity of CuNPs−EG nanofluid system. In this method, calculations of the thermal conductivity (*k*) were conducted using the following Green−Kubo formula [49]:

$$k = \frac{V}{3k_B T^2} \int \left\langle \vec{J}(0) \cdot \vec{J}(t) \right\rangle dt \tag{3}$$

where *V*, *T*, k_B and *J(t)* represent the simulation box volume, the temperature of the system, Boltzmann constant and the heat flux, respectively. The angular brackets in equation 3 represent the average over all atoms in the CuNPs−EG simulation domain. Additionally, the heat flux *J(t)* can be expanded to equation 4 [50]:

$$\vec{J}(t) = \frac{1}{V}\sum_{i}\left[\left(E_{k,i} + E_{p,i} - \langle h_i \rangle\right)\vec{v}_i + \sum_{j,j\neq i}(\vec{f}_{ij}\cdot\vec{r}_{ij})\vec{v}_j\right] \tag{4}$$

where $E_{k,i}$ and $E_{p,i}$ are the kinetic energy and potential energy of the i^{th} atom; $\vec{f}_{ij}$ is the force applied on the i^{th} atom from the j^{th} atom; $\vec{r}_{ij}$ is the distance between i^{th} and j^{th} atoms; $\vec{v}_i$ and $\vec{v}_j$ are velocities of the i^{th} and j^{th} atoms, respectively. The average enthalpy $\langle h_i \rangle$ of the i^{th} atom can be computed using [51]:

$$\langle h_i \rangle = \langle E_{k,i} \rangle + \langle E_{p,i} \rangle \tag{5}$$

In this study, the numerical calculations were performed for discrete molecular dynamics (MD) with time steps length Δt, hence, Eq.3 is calculated as [52].

$$k = \frac{\Delta t}{3Vk_B T^2}\sum_{m=1}^{M}\frac{1}{N-m}\sum_{n=1}^{N-m}J(m+n)J(n) \tag{6}$$

where *N* is the total number of time steps of the simulation, and *M* is the number of time steps for the correlation of heat flux vectors. The heat flux autocorrelation function (HFACF) is represented by the outer summation in Eq. 6.

2.4. Experimental measurements of CuNPs-EG nanofluid thermal conductivity

Recently, a variety of thermal conductivity measurement techniques were developed for solid and liquid materials with a broad temperature range [53]. For thermal conductivity analysis of nanofluids, transient hot wire, steady state parallel plate method, laser flash diffusivity method, and the conventional 3ω method are most used [54]. In this work, the thermal conductivity of nanofluids was measured through a modified homemade steady-state

method where a cylindrical cell was used as shown in figure 3. The fabricated CuNPs-EG nanofluid was placed in the annular space between the long vertical concentric cylinders made with copper. The cylindrical configuration of the system allows a uniform heat flux in the radial direction when the internal hot cylinder is heated electrically to the desired temperature. The generated unidirectional heat flux will flow continuously to the external cold cylinder through the nanofluid. In addition, the operating temperature of the system was controlled by a temperature controller which was installed at the outer side of the cold cylinder (figure 3). The system was isolated by a thermal insulating material to reduce heat losses to the surrounding air. The effective thermal conductivity (*k)* of the fabricated nanofluid was calculated using the one-dimensional heat conduction equation [55]:

$$Q = \frac{kA}{d}(T_h - T_c) \tag{7}$$

where Q is the heat flux (it is equal to the power supplied by a power supply to the hot cylinder), A is the lateral area of the hot cylinder, d is the distance between the hot and cold cylinders, T_h is the temperature of the hot cylinder, T_c is the temperature of the cold cylinder.

To produce accurate results, the experimental apparatus was calibrated by measuring the thermal conductivity of deionized water (k_d) in the temperature range of 298 to 318 K (Table 2). The measured k_d values were compared with references k_{dR} data using the correction factor (F) defined by equation 8:

$$F = \frac{k_{dR}}{k_d} \tag{8}$$

All the obtained values of EG and CuNPs-EG nanofluid thermal conductivity were multiplied by the correction factor F for each temperature for accuracy improvement.

Table 2 Correction factor (F) values at different temperatures after the experimental water thermal conductivity comparison with the reference [55].

Temperature (K)	Thermal conductivity (reference k_{dR})	Thermal conductivity (this study k_d)	Correction factor (F)
298	0.61058	0,7395	0,825666
303	0,61827	0,745	0,829893
308	0,62692	0,763	0,821651
313	0,63558	0,8134	0,781387
318	0,64231	0,838	0,76648

3. Results and Discussions

3.1. Structural analysis of the fabricated CuNPs by X-ray diffraction

To confirm the crystalline structure of the fabricated nanoparticles, XRD analysis was conducted and is depicted in figure 4. It was clearly shown that the characteristic diffraction peaks of Cu located at 43.61°, 50.6°, and 74° were observed and compared to a Cu standard card (JCPDS 04-0836). They correspond to the (111), (200), and (220) planes of the fcc Cu structure, respectively [56]. No other impurities were detected in the samples. This result confirms that with the laser ablation process, it became possible to obtain pure CuNPs in EG without any additional hazardous chemicals. Indeed, no other nanostructures of Cu_2O or CuO were observed in the fabricated material. However, there is a possibility of oxides thin layers on the surface of the Cu nanoparticles which were not detectable in the XRD analysis, even at lower scanning speed. Possibly, the oxide layers were too thin and below the detection limit of the used XRD instrument [57].

3.2. Morphological analysis

TEM analysis of the fabricated CuNPs in EG was performed on a nanofluid sample

obtained after 5 mins ablation time (t_a). The low-magnification TEM micro-image (figure 5a) shows that the fabricated CuNPs-EG nanofluid is composed of Cu nanoparticles with an average diameter of around ~ 7 nm. The Cu nanoparticles are confirmed to be spherical in shape as highlighted in the high magnification TEM image (figure 5b). Furthermore, the selected area electron diffraction (SAED) pattern (figure 5c) of CuNPs is clearly showing rings that can be assigned to the various lattice planes of the face-centered cubic of Cu [58]. The CuNPs are much smaller in size when compared to the CuNPs prepared by other reported chemical methods [58-61]. In addition, figure 5d shows a particle size distribution histogram which was obtained from the TEM micrographs by counting approximately 540 Cu nanoparticles. The blue solid line corresponds to a log-normal fit distribution, which reveals an average particle size of 7 nm and a standard deviation σ = 0.33.

3.3. CuNPs and ethylene glycol (EG) MD-models: Radial distribution functions

For accuracy in our MD calculations, a united atomic representation was used to construct the CuNPs-EG nanofluid model system. The calculated radial distribution function (RDF) for the CuNP and EG base fluid at T = 298 K are shown in figures 6a and 6b, respectively. We can confirm the existence of solid Cu and EG liquid as expected. The structure of the solid Cu has regular, periodic structures, and each peak has a slightly broadened shape which is caused by Cu atoms vibrating around their lattice sites. For EG ($C_2H_6O_2$) base fluid, the RDFs were calculated using both specific atoms (i.e., H-H and O-O) and the center of the mass of the CH_2 molecule since each EG molecule consists of six interaction sites, i.e., the oxygen atoms (O), the hydrogen atoms (H) of the hydroxyl groups, and the methylene (CH_2) groups [44]. CH_2 are considered as single interaction sites with their centers located at the position of the carbon (C) atoms [49]. From figure 6.b, it is observed that the first peaks for the RDF of H, O and CH_2 are the sharpest, which indicates the first coordination sphere of the EG liquid.

Otherwise, the EG as a liquid, which is illustrated in the inset of Figure 6.b, does not maintain a constant molecular arrangement and loses all of its long-range atomic structure. The molecules become independent of each other, and the distribution returns to the bulk density where g(r) = 1 which confirms the liquid nature of the used EG model [44,49].

3.4. Thermal conductivity analysis of CuNPs-EG nanofluid: MD simulations vs experimental data

3.4.1. Validation of EMD-GK model for thermal conductivity analysis of pure EG-base fluid

To validate the simulation method, EMD simulations integrated with Green-Kubo (EMD-GK) method was used to count the thermal conductivity (*k*) value of the single-phase EG base fluid (10,000 atoms), as well as to compare it with the available experimental and numerical data in the literature at standard conditions (T = 298 K and P = 1 atm). By using equation 6, thermal conductivity (*k*) of the EG base fluid could be calculated with an acceptable margin of error. However, the area under the converged heat flux autocorrelation function (HFACF) overtime should be analyzed (figure 7). For accuracy in EMD-GK calculations, the HFACF function must decay to zero within the integral time length [49]. From figure 7, the oscillating HFACF for EG decayed monotonically where the required time to decay to zero was estimated to be around 15,000 fs correlation time at T = 298 K. From this result, it is observed that the fluctuations of the heat flux of the EG base fluid system were gradually damped, which leads to an excellent integral of the HFACF. Moreover, the uniform behavior of the HFACF after 15,000 fs correlation time could be caused by the freedom of movement of the EG molecules which have strong cohesion among different degrees of freedom (e.g., rotational and transitional).

The thermal conductivity (*k*) of the base fluid (EG) was evaluated from the HFACF by the average of the integrands between 15,000 and 20,000 fs when the oscillations are smaller

[45]. *k* was obtained from the average of five independent runs of the same EG system. The deviation of each run was less than ± 0.006 W/mK and the deviation of five independent runs was less than ± 0.008 W/mK. The obtained result was equal to k = 0.252 W/mK, which is consistent with various reported numerical simulation values [49,62] and it is comparable to the experimental value obtained in this study (0.27 W/mK) for EG base fluid. These results confirmed the suitability of using this EMD-GK method to predict and to study thermo-physical properties in more complex systems such as CuNPs-EG based nanofluids.

3.4.2. MD simulations vs experimental thermal conductivity for CuNPs-EG nanofluid

In the present study, in addition to the MD-based simulation method, an experimental technique (i.e., guarded hot-plate) was further used to investigate the thermal conductivity (*k*) of CuNPs-EG nanofluid obtained at a relatively short ablation time t_a = 5 mins. The results were compared with the values calculated computationally. The thermal conductivity (*k*) values were recorded at different temperatures, ranging from 298 to 318 K as shown in figure 8. From these results, it can be seen that a linear increase in the thermal conductivity with the base fluid and nanofluid temperatures was observed with trends showing almost similarities for the experimentally measured and the predicted values by the used equilibrium molecular dynamics (EMD) simulations integrated with Green-Kubo method (EMD-GK). The small discrepancies between both values, numerical and experimental, could be originated from the different diameters and shapes of CuNPs obtained experimentally (as shown in the TEM micro-images, figure 5. a and b) than those of the modeled CuNPs in the MD simulation as shown in the inset of figure 6.a. This could lead to a degree of difference between the experimental data and simulation results [30,34]. Moreover, other possible factors during the fabrication process of CuNPs-EG nanofluid could be the reason for these slight deviations, such as the defects in the CuNPs created during the laser ablation. In our study, these factors

weren't taken into account during the thermal conductivity numerical calculations. However, the MD simulations of the thermal conductivity of the fabricated CuNPs-EG nanofluids are in good agreement with experimental data, particularly at temperatures above 308 K. Additionally, varying the temperature also showed a slight deviation from a linear increase in thermal conductivity with temperature. This could be related to nanoparticle clustering effects which could cause precipitation. The enhancement η(%) in thermal conductivity is represented as a percentage deviation in thermal conductivity of the nanofluids (k_{nf}) against the base fluid (k_b), and it could be calculated by using the following equation:

$$\eta(\%) = 100 \times \frac{(k_{nf} - k_b)}{k_b} \tag{9}$$

The relative enhancement (η) in the percentage of thermal conductivity of CuNPs-EG nanofluids obtained after 5 mins ablation time (t_a) was calculated by equation (9) and plotted as a function of temperature (figures 9.a). The average enhancement at 318 K was found to be around 15%, while the value obtained numerically was 18%. These obtained results for the thermal conductivity enhancement of CuNPs-EG nanofluids at higher temperatures may become more pronounced if the nanoparticles' diffusion in the liquid is enhanced by the addition of surfactants to reduce the clustering effects of the nanoparticles [63,64]. Moreover, the ablation time (t_a) is a critical parameter since the concentration of CuNPs in EG depends greatly on it, and by controlling the ablation time, the CuNPs-EG nanofluid could be tailored to fit any applications where high-performance heat transfer fluids are required. Therefore, the relative enhancement (η) was also investigated experimentally for samples obtained at 5, 10, 20, and 30 mins as shown in figure 9.b. It was observed that the enhancement was higher (~ 24%) as the ablation time was extended to 30 mins. Compared with our previous work on Al_2O_3-H_2O nanofluid [55], it was found that its thermal conductivity enhancement (8.6%) was lower than CuNPs-EG which confirms the high performance and suitability of this

material as advanced heat transfer fluid for different industrial applications. The better performance of CuNPs-EG obtained after 30 mins ablation time indicates the dependence of thermal conductivity of the suspensions on temperature as well as the ablation time which has a direct effect on the volume concentration of Cu nanoparticles in the base fluid.

4. Conclusion

In the present study, copper nanoparticles in ethylene glycol (CuNPs-EG) based nanofluid were prepared by pulsed ND-YAG (λ = 1064 nm) laser ablation of bulk copper target in EG base-fluid at a pulse duration of 20 ns. Thermal conductivity (k) analysis was carried out by using a computational approach based equilibrium molecular dynamics (EMD) simulations integrated with Green-Kubo (EMD-GK) method. The EMD-GK results for k were confirmed experimentally through a homemade steady-state apparatus at different temperatures (T) ranging from 298 K to 318 K. The effect of ablation time (t_a) on the thermal conductivity performance of CuNPs-EG nanofluid was also investigated. Interestingly, the relative enhancement in thermal conductivity was higher as T and t_a increased, in particular for samples obtained after t_a = 30 mins. The relative enhancement (η) in the percentage of thermal conductivity of CuNPs-EG nanofluids obtained after t_a = 5 mins was 15% at 318 K, while samples obtained after t_a = 30 mins showed an enhancement of 24% in thermal conductivity. Similar to the results obtained from the experimental method, the EMD-GK simulations of thermal conductivity also increased with increasing T which confirmed the suitability of using the MD approach in predicting and designing nanofluids with good thermo-physical properties and heat transfer performance. The results obtained in the present study showed the advantage of using a laser based ablation method to fabricate highly efficient CuNPs-EG nanofluid which could be used as an alternative for heat transfer applications, in particular for solar thermal engineering systems and electronics cooling.

Acknowledgements

This work is based on the research supported in part by the National Research Foundation (NRF) of South Africa (Grant number: 115886); and the UNESCO-UNISA Africa Chair in nanoscience and nanotechnology. Part of the work was also supported by the Nanosciences African Network (NANOAFNET)-iThemba LABS, Nanoenergy for Sustainable Development in Africa (NESDAF) and the School of Physics and Chemistry at UKZN.

References

[1] I. Khan, K. Saeed, I. Khan, Nanoparticles: Properties, applications and toxicities, Arab. J. Chem. 12 (7) (2019) 908-931, https://doi.org/10.1016/j.arabjc.2017.05.011.

[2] P.P. Murmu, A. Shettigar, S.V. Chong, Z. Liu, D. Goodacre, V. Jovic, T. Mori, K.E. Smith, J. Kennedy, Role of phase separation in nanocomposite indium-tin-oxide films for transparent thermoelectric applications, J. Materiomics. In Press, (2020), https://doi.org/10.1016/j.jmat.2020.10.015

[3] P.P. Murmu, V. Karthik, Z. Liu, V. Jovic, T. Mori, W.L. Yang, K.E. Smith, J.V. Kennedy, Influence of Carrier Density and Energy Barrier Scattering on a High Seebeck Coefficient and Power Factor in Transparent Thermoelectric Copper Iodide, ACS Appl. Energy Mater. 3 (2020) 10037-10044, https://doi.org/10.1021/acsaem.0c01724

[4] R. Saidur, K.Y. Leong, H.A. Mohammad, A review on applications and challenges of nanofluids, Renew. Sust. Energ. Rev. 15 (3) (2011) 1646-1668, https://doi.org/10.1016/j.rser.2010.11.035.

[5] J. Buongiorno, D.C. Venerus, N. Prabhat, T. McKrell, J. Townsend, R. Christianson, Y.V. Tolmachev, P. Keblinski, L.W. Hu, J.L. Alvarado, I.C. Bang, A benchmark study on the thermal conductivity of nanofluids, J. Appl. Phys. 106 (2009), 094312, https://doi.org/10.1063/1.3245330

[6] S. Iyahraja, J.S. Rajadurai, Study of thermal conductivity enhancement of aqueous suspensions containing silver nanoparticles, AIP Adv. 5 (5) (2015) 057103, https://doi.org/10.1063/1.4919808.

[7] T. Khamliche, S. Khamlich, T.B. Doyle, D. Makinde, M. Maaza, Thermal conductivity enhancement of nano-silver particles dispersed ethylene glycol based nanofluids, Mater. Res. Express. 3 (2018) 035020, https://doi.org/10.1088/2053-1591/aab27a.

[8] M.C. Mbambo, S. Khamlich, T. Khamliche, B.M. Mothudi, M. Maaza, Pulsed Nd:YAG laser assisted fabrication of graphene nanosheets in water, MRS Adv. 3 (42) (2018) 2573-2580, https://doi.org/10.1557/adv.2018.275.

[9] C.H. Chon, K.D. Kihm, Thermal conductivity enhancement of nanofluids by brownian motion, J. heat transfer. 127 (8) (2005) 810, https://doi.org/10.1115/1.2033316.

[10] C. Kleinstreuer, Y. Feng, Experimental and theoretical studies of nanofluid thermal conductivity enhancement: A review, Nanoscale Res. Lett. 6 (1) (2011) 229, https://doi.org/10.1186/1556-276X-6-229.

[11] T.S. Ahmadi, Z.L. Wang, T.C. Green, A. Henglein, M.A. El-Sayed, Shape controlled synthesis of colloidal platinum nanoparticles, Science 272 (5270) (1996) 1924-1925, https://doi.org/10.1126/science.272.5270.1924.

[12] H.H. Huang, X.P. Ni, G.L. Loy, C.H. Chew, K.L. Tan, F.C. Loh, J.F. Deng, G.Q. Xu, Photochemical formation of silver nanoparticles in poly(N vinylpyrrolidone), Langmuir 12 (4) (1996) 909–912, https://doi.org/10.1021/la950435d.

[13] R.A. Haydarov, R.R. Khaydarov, O. Gapurova, Y. Estrin, T. Schepe, Electrochemical method for the synthesis of silver nanoparticles, J Nanopart Res. 11 (5) (2009) 1193-1200, https://doi.org/10.1007/s11051-008-9513-x.

[14] C.Q. Chen, Q. Shen, H. Gao, Formation of nanoparticles in water in-oil micro emulsions controlled by the yield of hydrated electron: The controlled reduction of Cu2+, J. Colloid Interface Sci. 308 (2) (2007) 491-499, https://doi.org/10.1016/j.jcis.2006.12.021.

[15] R.T. Mendieta, R. Mondragón, V.P. Belda, O.M. Yero, J.J. Lancis, J.E. Juliá, G. MínguezVeg, Characterization of tin/ethylene glycol solar nanofluids synthesized by femtosecond laser radiation, ChemPhysChem. 18 (9) (2016) 1055-1060, https://doi.org/10.1002/cphc.201601083.

[16] D. Zhang, B. Gökce, S. Barcikowski, Laser synthesis and processing of colloids: Fundamentals and applications, Chem. Rev. 117 (5) (2017) 3990–4103, https://doi.org/10.1021/acs.chemrev.6b00468.

[17] P.P. Patil, D.M. Phase, S.A. Kulkarni, S.V. Ghaisas, S.K. Kulkarni, S.M. Kanetkar, S.B. Ogale, V.G. Bhide, Pulsed-laser induced reactive quenching at liquid-solid interface: Aqueous oxidation of iron, Phys. Rev. Lett. 58 (3) (1987) 238-241,

https://doi.org/10.1103/PhysRevLett.58.238.

[18] R. Saidur, K.Y. Leong, H. Mohammad, A review on applications and challenges of nanofluids, Renew. Sust. Energ. Rev. 15 (3) (2011) 1646-1668, https://doi.org/10.1016/j.rser.2010.11.035.

[19] M.C. Sportelli, M. Izzi, A. Volpe, M. Clemente, R.A. Picca, A. Ancona, P.M. Lugarà, G. Palazzo, N. Cioffi, The pros and cons of the use of laser ablation synthesis for the production of silver nano-antimicrobials, Antibiotics, 7 (2018) 67, https://doi.org/10.3390/antibiotics7030067

[20] I. Ghiuță, D. Cristea, D. Munteanu, Synthesis methods of metallic nanoparticles-an overview, Bull. Transylv. Univ. Braşov. 10 (59) (2017) 133-140.

[21] M.A. Garcia, Surface plasmons in metallic nanoparticles: Fundamentals and applications, J. Phys. D Appl. Phys. 44 28 (2011) 283001, https://doi.org/ 10.1088/0022-3727/44/28/283001.

[22] D.I. Gordeychuk, V.N. Sorokoumov, V.N. Mikhaylov, M.S. Panov, E.M. Khairullina, M.V. Melnik, V.A. Kochemirovsky, I.A. Balova, Copper-based nanocatalysts produced via laser-induced ex situ generation for homo- and cross-coupling reactions, Chem. Eng. Sci. 227 (2020) 115940, https://doi.org/10.1016/j.ces.2020.115940.

[23] P.V. Kazakevich, V.V. Vorono, A.V. Simakin, G.A. Shafeev, Production of copper and brass nanoparticles upon laser ablation in liquid, Quantum Elec. 34 (10) (2004) 951-956, https://doi.org/10.1070/QE2004V034N10ABEH002756.

[24] M. Kole, T.K. Dey, Enhanced thermophysical properties of copper nanoparticles dispersed in gear oil, Appl. Therm. Eng. 56 (1-2) (2013) 45-53, https://doi.org/10.1016/j.applthermaleng.2013.03.022.

[25] S. Link, C. Burda, B. Nikoobakht, M.A. El-Sayed, Laser induced shape changes of colloidal gold nanorods using femtosecond and nanosecond laser pulses, J. Phys. Chem. B 104 (26) (2000) 6152–6163, https://doi.org/10.1021/jp000679t.

[26] S.I. Dolgaev, A.V. Simakin, V.V. Voronov, G.A. Shafeev, F.B. Verduraz, Nanoparticles produced by laser ablation of solids in liquid environment, Appl. Surf. Sci. 186 (1-4) (2002) 546-551, https://doi.org/10.1016/S0169-4332(01)00634-1.

[27] J. Nedersen, G. Chumanov, T.M. Cotton, Laser ablation of metals: A new method for preparing SERS active colloids, Appl. Spectrosc. 47 (12) (1993) 1959-1964, https://doi.org/10.1366/0003702934066460.

[28] H.S. Desarkar, P. Kumbhakar, A.K. Mitra, Effect of ablation time and laser fluence on the optical properties of copper nano colloids prepared by laser ablation technique, Appl. Nanosci. 2 (3) (2012) 285–291, https://doi.org/10.1007/s13204-012-0106-8.

[29] N. Ali, J.A. Teixeira, A. Addali, A review on nanofluids: Fabrication, stability, and thermophysical properties, J. Nanomater. 2018 (3-4) (2018) https://doi.org/10.1155/2018/6978130.

[30] F. Jabbari, S. Saedodin, A. Rajabpour, Experimental investigation and molecular dynamics simulations of viscosity of CNT-water nanofluid at different temperatures and volume fractions of nanoparticles, J. Chem. Eng. Data 64 (1) (2018) 262-272, https://doi.org/10.1021/acs.jced.8b00783.

[31] H. Zerradi, S. Ouaskit, A. Dezairi, H. Loulijat, S. Mizani, New Nusselt number correlations to predict the thermal conductivity of nanofluids, Adv. Powder. Technol. 25 (2014) 1124–1131, https://doi.org/10.1016/j.apt.2014.02.020

[32] C. Ferrari, B. Kaoui, V.S. L'vov, I. Procaccia, O. Rudenko, J.H.M ten Thije Boonkkamp, F. Toschi, Analytical modeling for heat transfer in sheared flows of nanofluids. Physical Review E. 86 (2012) 016302, https://doi.org/10.1103/PhysRevE.86.016302

[33] S. Merabia, S. Shenogin, L. Joly, P. Keblinski, J.L. Barrat, Heat transfer from nanoparticles: A corresponding state analysis, PNAS. 106 (2009) 15113-15118, https://doi.org/10.1073/pnas.0901372106

[34] F. Jabbari, A. Rajabpour, S. Saedodin, Thermal conductivity and viscosity of nanofluids: A review of recent molecular dynamics studies, Chem. Eng. Sci. 174 (2017) 67−81, https://doi.org/10.1016/j.ces.2017.08.034.

[35] B. Y. Cao, R. Y Dong, Molecular dynamics calculation of rotational diffusion coefficient of a carbon nanotube in fluid, J. Chem. Phys. 140 (3) (2013) 034703, https://doi.org/10.1063/1.4861661.

[36] A.S. Tascini, J. Armstrong, E. Chiavazzo, M. Fasano, P. Asinari, F. Bresme, Thermal transport across nanoparticle-fluid interfaces: The interplay of interfacial curvature and nanoparticle fluid interactions, Phys. Chem. Chem. Phys. 19 (4) (2017) 3244−3253, https://doi.org/10.1039/C6CP06403E.

[37] R. Zamiri, B.Z. Azmi, M.S. Husin, G. Zamiri, H.A. Ahangar, Z. Rizwan, Thermal diffusivity measurement of copper nanofluid using pulsed laser thermal lens technique, J. Eur. Opt. Soc.-Rapid Publ. 7 (2012) 12022- 5, https://doi.org/10.2971/jeos.2012.12022.

[38] M. Dell'Aglio, R. Gaudiuso, O. De Pascale, A. De Giacomo, Mechanisms and processes of pulsed laser ablation in liquids during nanoparticle production, Appl. Surf. Sci. 348 (2015) 4-9, https://doi.org/10.1016/j.apsusc.2015.01.082.

[39] M. Maaza, B.D. Ngom, S. Khamlich, J.B. Kana Kana, P. Sibuyi, D. Hamidi, S. Ekambaram, Valency control in $MoO_{3-\delta}$ nanoparticles generated by pulsed laser liquid solid interaction, J. Nanoparticle Res. 14 (2) (2012) 714, https://doi.org/10.1007/s11051-011-0714-3.

[40] W.L. Jorgensen, Optimized intermolecular potential functions for liquid alcohols, J. Phys. Chem. 90 (7) (1986) 1276–1284, https://doi.org/10.1021/j100398a015.

[41] Y.S. Lin, P.Y. Hsiao, C.C. Chieng, Roles of nanolayer and particle size on thermophysical characteristics of ethylene glycol-based copper nanofluids, Appl. Phys. Lett. 98 (15) (2011) 153105, https://doi.org/10.1063/1.3579522.

[42] M.P. Allen, D.J. Tildesley, Computer simulations of liquids, Oxford University Press; 2nd edition, 2017, https://doi.org/10.1093/oso/9780198803195.001.0001.

[43] A. Rajabpour, F.Y. Akizi, M.M. Heyhat, K. Gordiz, Molecular dynamics simulation of the specific heat capacity of water-Cu nanofluids, Int. Nano Lett. 3 (1) (2013) 58, https://doi.org/10.1186/2228-5326-3-58.

[44] A. Kaiser, O. Ismailova, A. Koskela, S.E. Huber, M. Ritter, B. Cosenza, W. Benger, R. Nazmutdinov, M. Probst, Ethylene glycol revisited: Molecular dynamics simulations and visualization of the liquid and its hydrogen-bond network, J. Mol. Liq. 189 (100) (2014) 20-29, https://doi.org/10.1016/j.molliq.2013.05.033.

[45] W.L. Jorgensen, D.S. Maxwell, J. Tirado-Rives, Development and testing of the OPLS all-atom force field on conformational energetics and properties of organic liquids, J. Am. Chem. Soc. 118 (45) (1996) 11225-11236, https://doi.org/10.1021/ja9621760.

[46] S. Plimpton, Lammps-Large-Scale Atomic/Molecular Massively Parallel Simulator, (2007) Available from: http:// lammps.sandia.gov/.

[47] M. Morciano, M. Fasano, A. Nold, C. Braga, P. Yatsyshin, D.N. Sibley, B.D. Goddard, E. Chiavazzo, P. Asinari, S. Kalliadasis, Nonequilibrium molecular dynamics simulations of nanoconfined fluids at solid-liquid interfaces, J. Chem. Phys. 146 (24) (2017) 244507, https://doi.org/10.1063/1.4986904.

[48] Z. Lou, M. Yang, Molecular dynamics simulations on the shear viscosity of Al_2O_3 nanofluids, Comput Fluids. 117 (2015) 17−23, https://doi.org/10.1016/j.compfluid.2015.05.006 Fluids 2015.

[49] Y. S. Lin, P. Y. Hsiao, C. C. Chieng, Constructing a force interaction model for thermal conductivity computation using molecular dynamics simulation: Ethylene glycol as an example, J. Chem. Phys. 134 (15) (2011) 154509, https://doi.org/10.1063/1.3578184.

[50] H. Zerradi, H. Loulijat, Numerical simulation of thermal conductivity of aqueous nanofluids containing graphene nanosheets using molecular dynamics simulation, MOJABB 2 (6) (2018) 313–322, https://doi.org/10.15406/mojabb.2018.02.00087.

[51] R. Essajai, A. Mzerd, N.Hassanain, M. Qjani, Thermal conductivity enhancement of nanofluids composed of rod-shaped gold nanoparticles: Insights from molecular dynamics, J. Mol. Liq. 293 (2019) 111494, https://doi.org/10.1016/j.molliq.2019.111494.

[52] H. Matsubara, G. Kikugawa, M. Ishikiriyama, S.Yamashita, T. Ohara, Microscopic picture of heat conduction in liquid ethylene glycol by molecular dynamics simulation: Difference from the monohydric case, Int. J. Heat Mass Transf. 121 (2018) 1033-1038, https://doi.org/10.1016/j.ijheatmasstransfer.2018.01.060.

[53] L. Qiu, N. Zhu, Y. Feng, E.E. Michaelides, G. Żyła, D. Jing, X. Zhang, P.M. Norris, C.N. Markides, O. Mahian, O, A review of recent advances in thermophysical properties at the nanoscale: From solid state to colloids, Phys. Rep. 843 (2020) 1-81, https://doi.org/10.1016/j.physrep.2019.12.001.

[54] M.M. Tawfik, Experimental studies of nanofluid thermal conductivity enhancement and applications: A review, Renew. Sust. Energ. Rev. 75 (2017) 1239-1253, https://doi.org/10.1016/j.rser.2016.11.111.

[55] A. Riahi, S. Khamlich, M. Balghouthi, T. Khamliche, T.B. Doyle, W. Dimassi, A. Guizani, M. Maaza, Study of thermal conductivity of synthesized Al_2O_3-water nanofluid by pulsed laser ablation in liquid, J. Mol. Liq. 304 (2020) 112694, https://doi.org/10.1016/j.molliq.2020.112694.

[56] R. Betancourt-Galindo, P.Y. Reyes-Rodriguez, B.A. Puente-Urbina, C.A. Avila-Orta, O.S. Rodríguez-Fernández, G. Cadenas-Pliego, R.H. Lira-Saldivar, L.A. García-Cerda, Synthesis of ccopper nanoparticles by thermal decomposition and their antimicrobial properties, J. Nanomater. 5 (10) (2014) 1-5, https://doi.org/10.1155/2013/980545.

[57] M. Raja, J. Subha, F.B. Ali, S.H. Ryu, Synthesis of copper nanoparticles by electroreduction process, Mater. Manuf. Process. 8 (2008) 782-785, https://doi.org/10.1080/10426910802382080.

[58] M.B. Gawande, A. Goswami, F.X. Felpin, T. Asefa, X. Huang, R. Silva, X. Zou, R. Zboril, R.S. Varma, Cu and Cu-based nanoparticles: Synthesis and applications in catalysis, Chem. Rev. 116 (6) (2016) 3722-811, https://doi.org/10.1021/acs.chemrev.5b00482.

[59] K. Hina, S. Shamaila, Z. Nosheen, S. Rehana, N. Jawad, R. Mohammad, G. Sheeba, S. Hussain, Antibacterial behavior of laser-ablated copper nanoparticles, Acta Metall Sin-Engl. 29 (8) (2016) 748–754, https://doi.org/10.1007/s40195-016-0450-x.

[60] Z. Tang, M. Hasegawa, Y. Nagai, M. Saito, Density functional study on metastable bcc copper: Electronic structure and momentum density of positron-electron pairs, Phys. Rev. B Condens. Matter 65 (19) (2002), https://doi.org/10.1103/PhysRevB.65.195108.

[61] A.S. Razium, T.H.S. Syed, Sirajuddin, M. Najma, R.S. Mohammad, H.K. Nazar, R.H. Keith, S. Afzal, Synthesis of air stable copper nanoparticles and their use in catalysis, Adv. Mater. Lett. 5 (4) (2014) 191-198, https://doi.org/10.5185/amlett.2013.8541.

[62] R. DiGuilio, A.S. Teja, Thermal conductivity of poly (ethylene glycols) and their binary mixtures, J. Chem. Eng. Data 35 (1990) 117-121, https://doi.org/10.1021/je00060a005.

[63] M.C. Mbambo, S. Khamlich, T. Khamliche, M.K. Moodley, K. Kaviyarasu, I.G. Madiba, M.J. Madito, M. Khenfouch, J. Kennedy, M. Henini, E. Manikandan, Remarkable thermal conductivity enhancement in Ag-decorated graphene nanocomposites based nanofluid by laser liquid solid interaction in ethylene glycol. Sci. Rep. 10 (2020) 1-14, https://doi.org/10.1038/s41598-020-67418-3.

[64] G. Xia, H. Jiang, R. Liu, Y. Zhai, Effects of surfactant on the stability and thermal conductivity of Al_2O_3/de-ionized water nanofluids, Int. J. Therm. Sci. 84 (2014) 118–124, https://doi.org/10.1016/j.ijthermalsci.2014.05.004.

Figure captions

Figure 1 Possible mechanisms causing the ablation of solid materials (Cu) in liquids (EG*)*.

Figure 2 CuNP-EG nanofluid molecular dynamic model with periodic boundary conditions in a 3D-computing domain: CuNP with diameter 7 nm, and surrounding EG molecules in the simulation box with dimensions of 100 Å × 100 Å × 100 Å (volume fraction of 1%) in a 3 dimensional (3D) view.

Figure 3 Schematic description of a cylindrical cell for steady-state thermal-conductivity measurement of nanofluids

Figure 4 X-ray diffraction of CuNPs fabricated by laser ablation in EG.

Figure 5 (a,b) TEM micro-images of the prepared CuNPs by pulsed laser ablation in EG, (c) Selected area electron diffraction (SAED), and (d) Particle Size Distribution of CuNPs.

Figure 6 Radial distribution functions (RDFs) for (a) copper nanoparticle CuNP, and (b) EG base fluid (inset: EG molecule and the EG MD model).

Figure 7 Computed heat flux autocorrelation functions for EG base fluid at T = 298 K and P = 1 atm.

Figure 8 Measured and computed thermal conductivities of EG base-fluid and CuNPs-EG nanofluid (t_a = 5 mins) at different temperatures.

Figure 9 (a) Relative enhancements η(%) of CuNPs-EG nanofluid at different temperatures, and (b) at different ablation times.

Figures

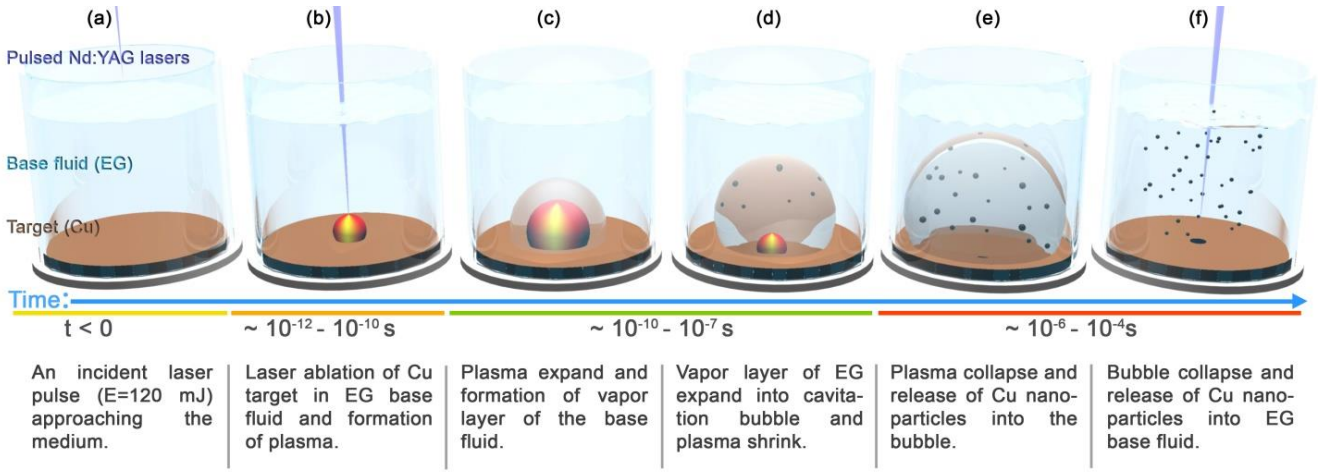

Figure 1

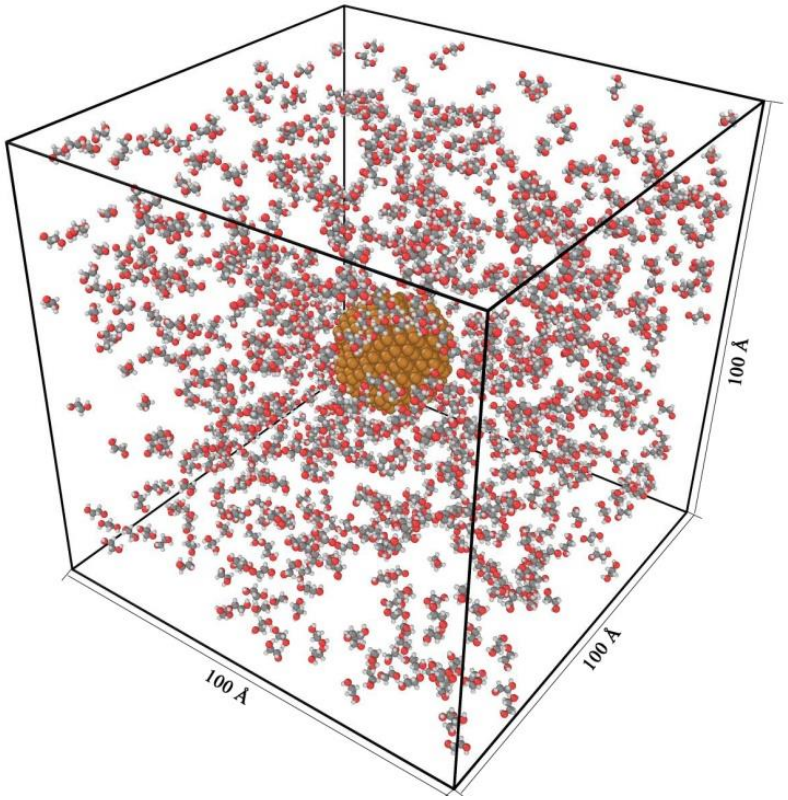

Figure 2

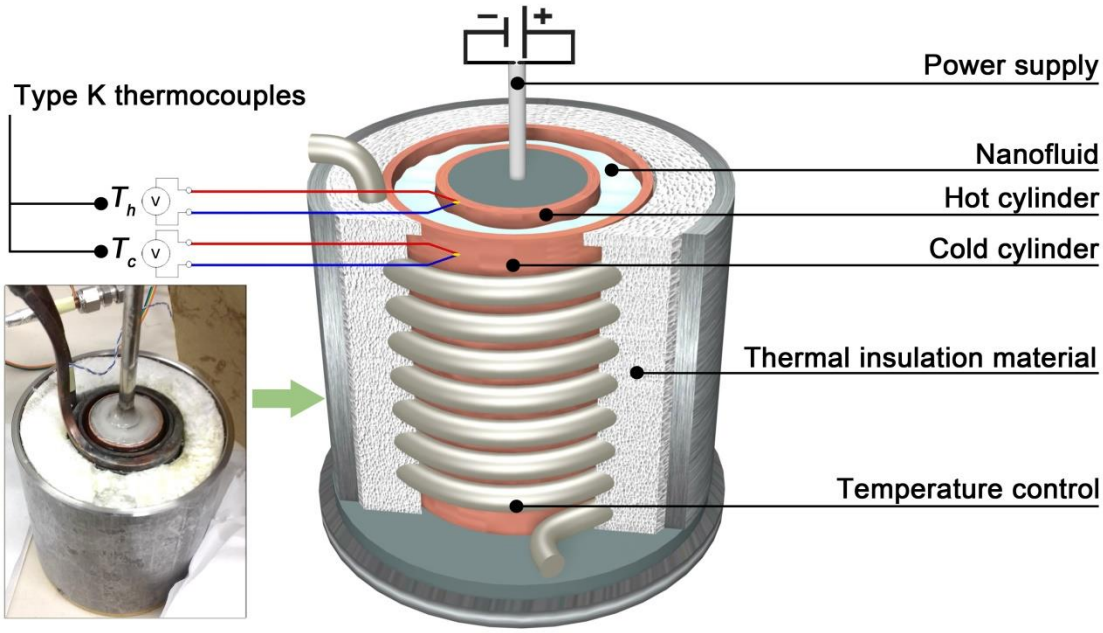
Type K thermocouples
T_h
T_c
V
V
Power supply
Nanofluid
Hot cylinder
Cold cylinder
Thermal insulation material
Temperature control

Figure 3

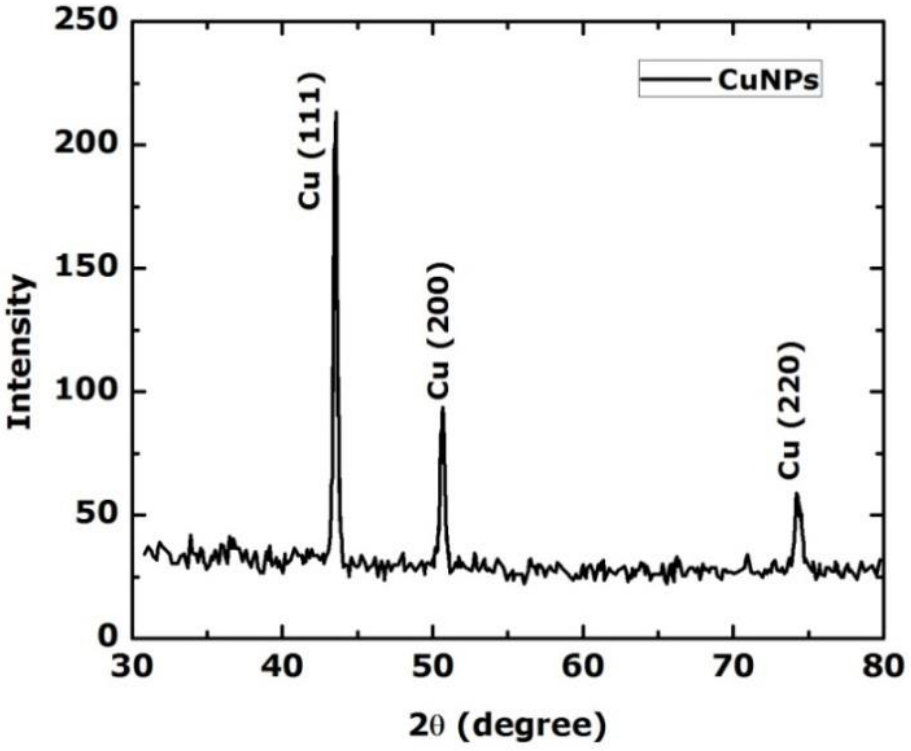
CuNPs
Cu (111)
Cu (200)
Cu (220)
Intensity
2θ (degree)
0
50
100
150
200
250
30
40
50
60
70
80

Figure 4

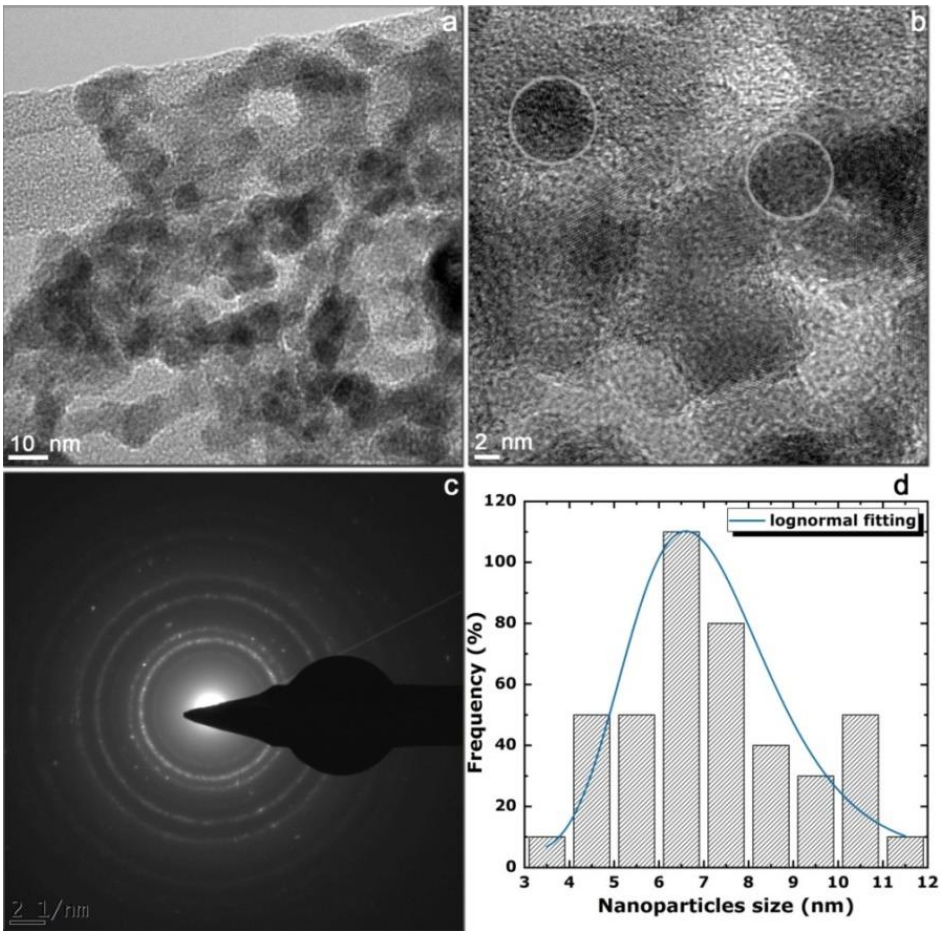
a
10 nm
b
2 nm
c
2 1/nm
d
lognormal fitting
Frequency (%)
Nanoparticles size (nm)
0
20
40
60
80
100
120
3
4
5
6
7
8
9
10
11
12

Figure 5

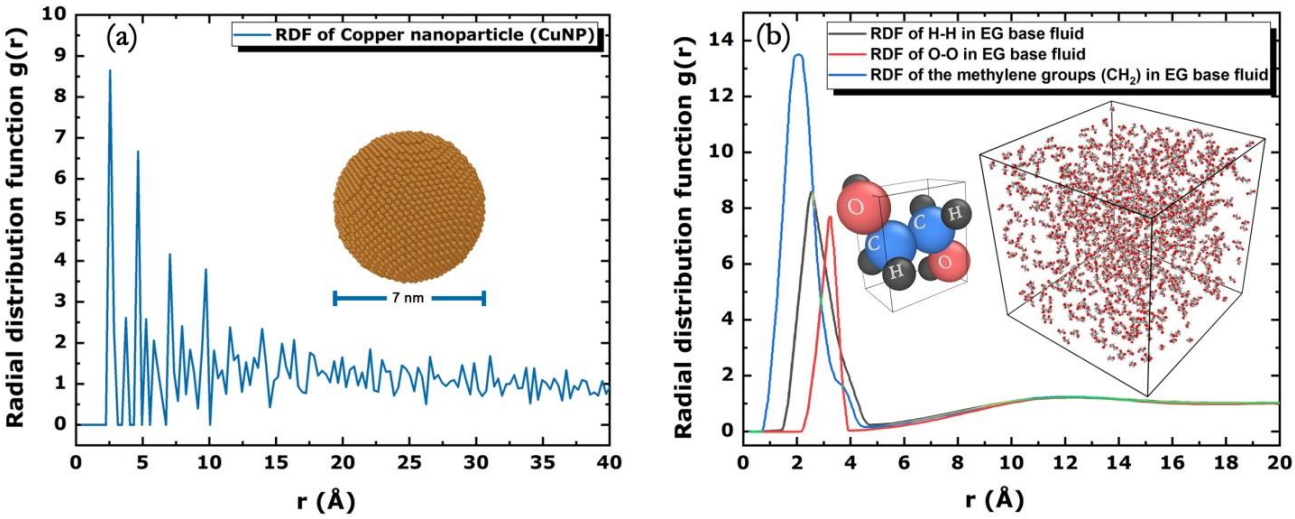
(a)
RDF of Copper nanoparticle (CuNP)
7 nm
Radial distribution function g(r)
r (Å)
(b)
RDF of H-H in EG base fluid
RDF of O-O in EG base fluid
RDF of the methylene groups (CH2) in EG base fluid
O
C
H
C
H
O
Radial distribution function g(r)
r (Å)

Figure 6

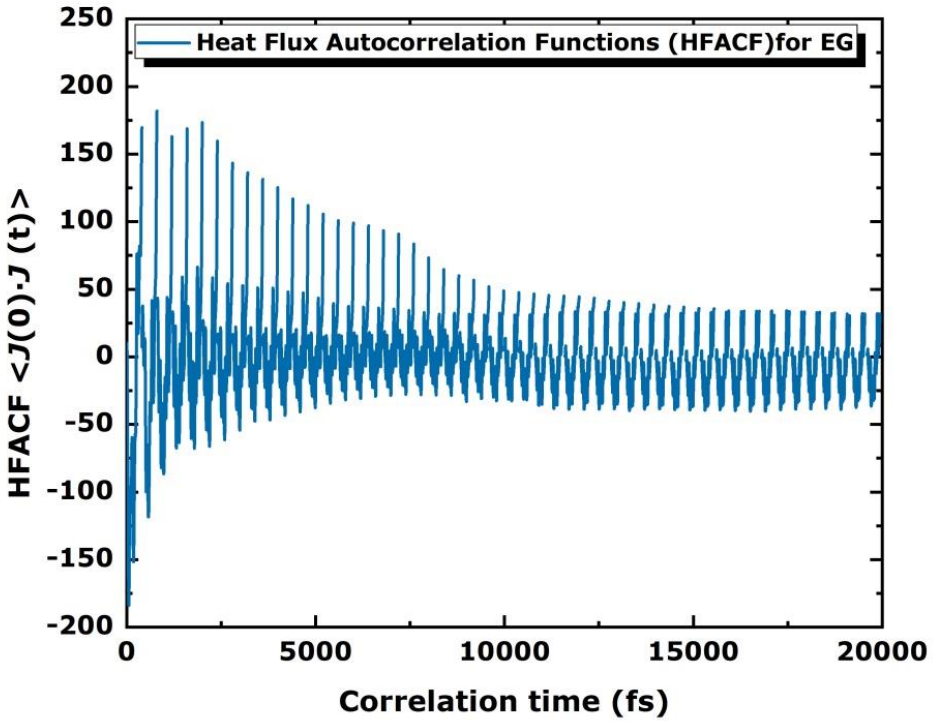
Heat Flux Autocorrelation Functions (HFACF)for EG
HFACF <J(0)·J (t)>
Correlation time (fs)
250
200
150
100
50
0
-50
-100
-150
-200
0
5000
10000
15000
20000

Figure 7

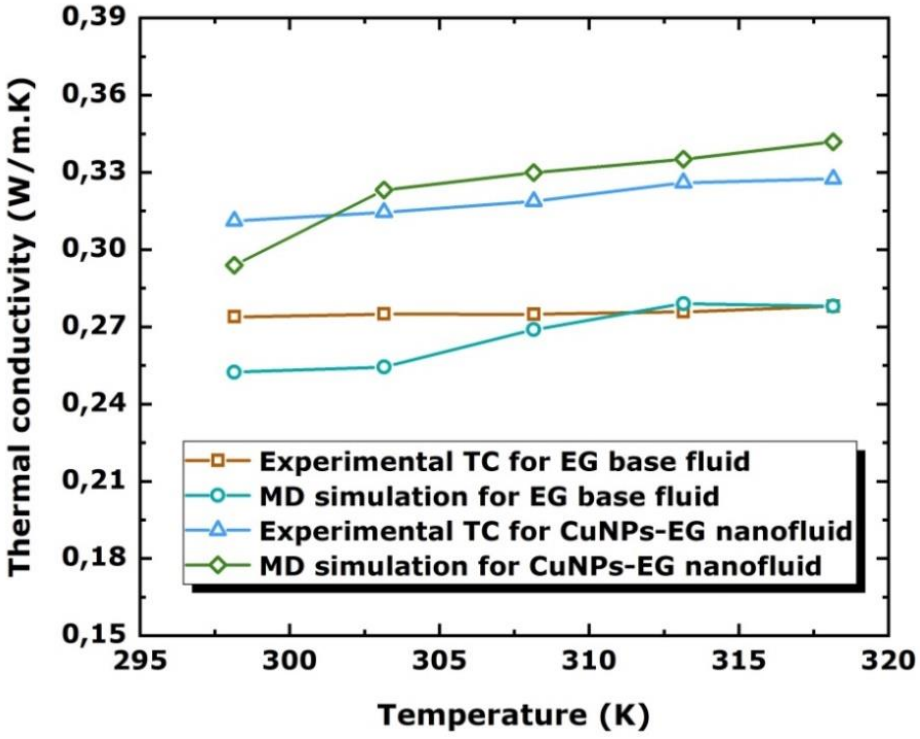
Thermal conductivity (W/m.K)
0,39
0,36
0,33
0,30
0,27
0,24
0,21
0,18
0,15
295
300
305
310
315
320
Temperature (K)
Experimental TC for EG base fluid
MD simulation for EG base fluid
Experimental TC for CuNPs-EG nanofluid
MD simulation for CuNPs-EG nanofluid

Figure 8

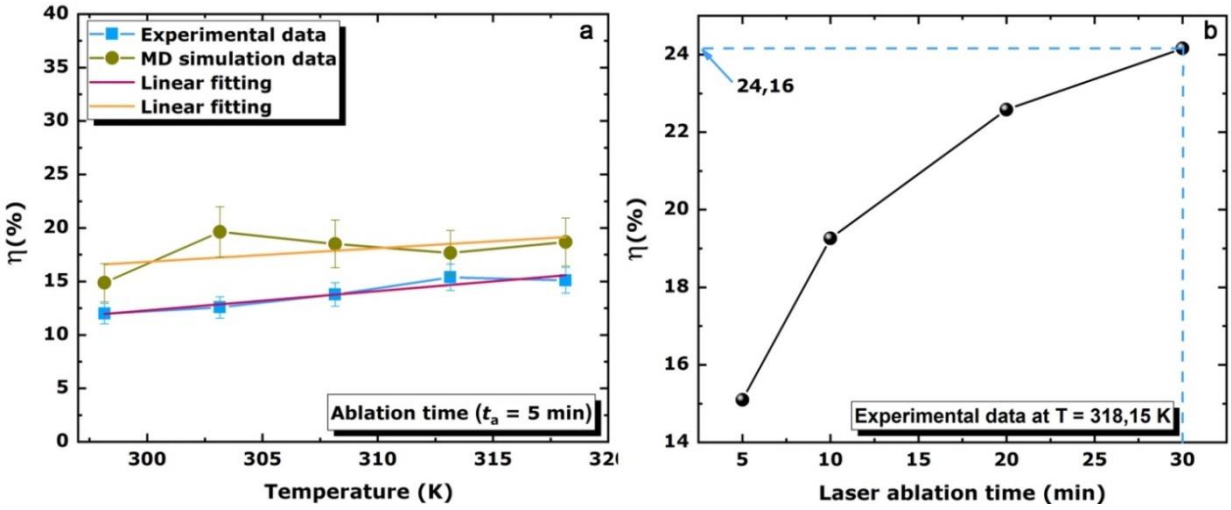
a
Experimental data
MD simulation data
Linear fitting
Linear fitting
Ablation time (t_a = 5 min)
η(%)
Temperature (K)
b
24,16
Experimental data at T = 318,15 K
η(%)
Laser ablation time (min)

Figure 9